Investigation of evaporation and condensation processes specific to grooved flat heat pipes

S. Lips, Jocelyn Bonjour, Frédéric Lefevre

Frontiers in Heat Pipes (FHP), 1, 023001 (2010)
DOI: 10.5098/fhp.v1.2.3001

Global Digital Central
ISSN: 2155-658X

Frontiers in Heat Pipes

Available at www.ThermalFluidsCentral.org

INVESTIGATION OF EVAPORATION AND CONDENSATION PROCESSES SPECIFIC TO GROOVED FLAT HEAT PIPES

Stéphane Lips, Jocelyn Bonjour, Frédéric Lefèvre*

Université de Lyon, CNRS
INSA-Lyon, CETHIL, UMR5008, F-69621, Villeurbanne, France
Université Lyon 1, F-69622, France

ABSTRACT

Temperature and liquid-vapor interface measurements obtained with a flat plate heat pipe (FPHP) in various experimental conditions are presented. The grooved FPHP is made of copper. The results are compared to a thermal model, developed in a previous work, in which heat conduction in the FPHP wall as well as evaporation and condensation heat transfer phenomena are taken into account. The model depends on the shape of the liquid-vapor interface in the grooves and on the fins at the condenser. A good agreement is found between the evaporation model and the experimental data. However the results of the condensation model overestimate the heat transfer coefficient, due to a bad estimation of the condensate film on the fins. Experimental measurements obtained with a second FPHP made of silicon are used to analyze the shape of this film. For both evaporation and condensation models, the results show a strong influence of the accommodation coefficient.

Keywords: *meniscus curvature radius, thermal model, accommodation coefficient, condensate film*

1. INTRODUCTION

Flat plate heat pipes (FPHP) have been widely studied in the last fifteen years, especially for their application to electronic cooling (Lallemand *et al.*, 2004; Vasiliev *et al.*, 2008). Although the literature on FPHP is abundant, experimental studies are relatively rare and do not provide measurements inside these systems, but only surface temperature measurements. Theoretical models are based on previous works developed for micro heat pipes. Among these articles, the model of Longtin *et al.* (1994) has been the basis of numerous other hydrodynamic models, which are based on the Young-Laplace law and the balance equations. These models describe the liquid and vapor pressures and velocities, as well as the meniscus curvature radius and thus the shape of the liquid inside the micro heat pipe. These models can be similarly developed for grooved capillary structures of flat plate heat pipes.

In the recent year, we have developed experimental benches to validate such models using confocal microscopy (Rullière et al., 2007). Different grooved FPHP were closed with a transparent wafer to allow liquid-vapor interface measurements by confocal microscopy. The accuracy of this optical measurement technique permits to estimate the meniscus curvature radius along the heat pipe. In the literature, the boundary condition for the meniscus curvature radius at the condenser was often considered as infinite in the hydrodynamic model, since no model was available to calculate this parameter. Confocal microscopy has been useful to understand the influence of both the vapor space thickness and the filling ratio on this parameter (Lips et al., 2010).

Even though hydrodynamic aspects are fundamental to characterize and increase the limits of the systems, and especially the capillary limit, thermal aspects should not be neglected. Indeed, in normal working conditions, a FPHP must have a small thermal resistance to minimize the temperature difference between the heat sink(s) and the heat source(s). Some authors have developed refined thermal models of FPHP (Khrustalev and Faghri, 1999; Kim *et al.*, 2003; Lefèvre *et al.*, 2008). Similarly to the hydrodynamic models, thermal models are derived from micro heat pipe models (Khrustalev and Faghri, 1994 & 1995).

In FPHPs, evaporation and condensation heat transfer depend on the shape of the liquid-vapor interface. Furthermore, some models presented in the literature include physical parameters whose effects arise mostly in the very thin film at the junction between the wall and the meniscus like Van der Waals forces or the accommodation coefficient. The shape of the liquid-vapor in the grooves is provided by hydrodynamic models based on Young-Laplace law. At the evaporator, this shape is sufficient to model evaporation, since the top of the fins between the grooves is dry. At the condenser, condensation occurs principally at the top of the fins. Thus, this shape has to be evaluated to accurately predict heat transfer at the condenser.

In a previous article (Lefèvre *et al.*, 2008), we have presented a coupled hydrodynamic and thermal model of a grooved flat heat pipe. The accommodation coefficient was included in the model to calculate heat transfer coefficients at the liquid-vapor interface. A specific model was developed to calculate the shape of the condensate film on the fins. The complete model was compared to temperature measurements and meniscus curvature radii obtained by confocal microscopy. The FPHP was made of copper and filled with methanol. The application was the cooling of proton exchange membrane fuel cells. Thus, experimental conditions were not usual, with a wide evaporating area (190×90 mm^2) compared to the adiabatic area (10×90 mm^2) and the condenser area (30×90 mm^2). A good agreement was found between the experimental results and the model. Nevertheless, few experimental data were

* *Corresponding author. Email: Frederic.lefevre@insa-lyon.fr*

Global Digital Central
ISSN: 2155-658X

obtained because of the size of the FPHP. Furthermore, it was not possible to compare the theoretical shape of the condensate to experimental data, because it was not assessable with this FPHP.

In this article, we present liquid-vapor interface measurements and temperature measurements obtained with a FPHP of smaller dimensions. The FPHP, made of copper, is tested in various experimental conditions. The goal of the article is to confront the thermal model to new experimental data in order to check its validity. Since, the shape of the condensate film is still not assessable with this FPHP, we compare the shape calculated theoretically, to experimental date obtained recently with a FPHP made of silicon (Lefèvre *et al.*, 2010). Silicon reflects less incoming light than copper, which can explain the feasibility of the condensate film measurement by confocal microscopy.

2. THERMAL MODEL OF A FPHP WITH LONGITUDINAL GROOVES

A thermal model of a FPHP with longitudinal grooves is presented in this part. This model was already presented in a previous article (Lefèvre *et al.*, 2008). Besides, a modified version of the model is developed to estimate evaporation and condensation heat transfer coefficients through parameter estimation.

2.1 Nodal thermal model

In a FPHP, heat is transferred from the heat source to the heat sink by heat conduction in the wall and two-phase heat transfer at the evaporator and the condenser. These heat transfer phenomena are taken into account through different thermal resistances in the nodal model presented in Fig 1. The FPHP is divided into several control volumes for which the energy balance equation is written. The wall temperature T_i is calculated for each control volume i. At $x = 0$ and $x = L$, we assume that the FPHP is perfectly insulated. The boundary conditions on the FPHP wall are the following:

- uniform heat transfer q_{evap} rate imposed at the heat source
- heat flux equal to zero in the adiabatic zone
- uniform heat transfer rate q_{cond} at the heat sink

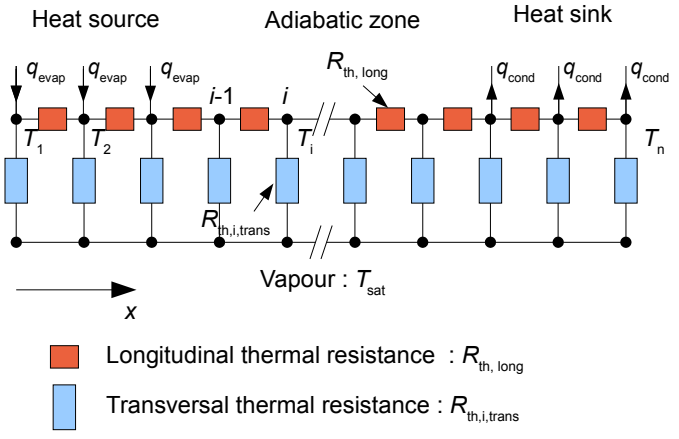

Fig.1 Nodal thermal model

Longitudinal heat conduction through the FPHP envelop is modeled by the thermal resistance $R_{th,long}$ that can be calculated considering the geometry of the FPHP (Lefèvre *et al.*, 2008) or estimated through a parameter estimation method by comparison of the model with temperature measurements obtained when the FPHP is empty. In that case, the transversal thermal resistances vanish from the model. Longitudinal thermal resistance is constant if we assume that the thermal conductivity of the FPHP envelop does not change significantly between the evaporator and the condenser.

Evaporation and condensation phenomena are modeled by transversal thermal resistances $R_{th,i,trans}$ which require specific models. The vapor temperature is assumed to be constant and equal to T_{sat}, which is verified since the pressure drop in the vapor is generally negligible. The energy balance in each control volume leads to a set of equations written as follows:

$$\frac{T_{i-1}+T_{i+1}}{R_{th,long}} - T_i\left(\frac{2}{R_{th,long}}+\frac{1}{R_{th,trans,i}}\right)+\frac{T_{sat}}{R_{th,trans,i}}+q_i=0 \qquad (1)$$

where the heat flux q_i is calculated as:

$$\begin{aligned} q_i &= q_{evap} = \frac{Q}{S_{evap}} \text{ at the evaporator} \\ q_i &= 0 \quad \text{in the adiabatic section} \\ q_i &= q_{cond} = \frac{-Q}{S_{cond}} \text{ at the condenser} \end{aligned} \qquad (2)$$

with Q the total heat transferred by the system. S_{evap} and S_{cond} are the evaporator surface and the condenser surface respectively.

2.2 Evaporator and condenser 2D models

Evaporator and condenser thermal models are presented in Fig.2. Since the cross section of the liquid flow in the grooves and the liquid velocity are small, liquid convection is negligible and heat transfer in the liquid is modeled by 2D heat conduction. The shape of the liquid-vapor interface in the capillary structure is supposed to be known. It can be either calculated using a hydrodynamic model (Lefèvre *et al.*, 2008) or determined experimentally (Rullière *et al.*, 2007).

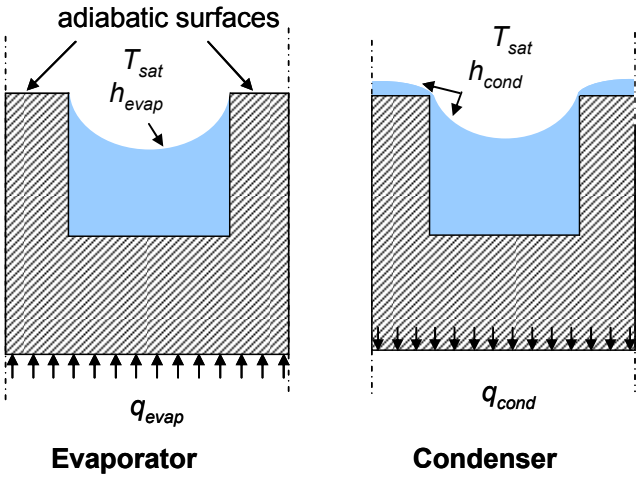

Fig. 2 Evaporator and condenser thermal models

In both evaporator and condenser models, a constant heat flux is applied at the external side of the wall. In the evaporator model, the top of the fins is assumed to be dry and thus an adiabatic condition is used since convection heat transfer between the wall and the vapor is negligible compared to evaporation heat transfer. On the contrary, condensation occurs mostly on the top of the fins because the thermal resistance of the condensate film is very small due to its small thickness. As a consequence, a hydrodynamic model has to be developed to calculate the condensate film shape on the top of the fin. This model is presented in next section.

Vertical boundaries are considered as adiabatic because of symmetries between the grooves. At the liquid-vapor interface a Fourier boundary condition is used to model evaporation and condensation

Global Digital Central
ISSN: 2155-658X

phenomena. Heat transfer coefficients h_{evap} and h_{cond} are calculated from the gas kinetic theory (Carey, 1992):

$$h_{evap} = h_{cond} = \frac{2a_c}{2-a_c}\frac{\rho_v h_{lv}^2}{T_{sat}}\frac{1}{\sqrt{2\pi\frac{R_g}{\overline{M}}T_{sat}}}\left(1-\frac{P_{sat}}{2\rho_v h_{lv}}\right) \quad (3)$$

where a_c is the accommodation coefficient, R_g the specific gas constant, $\overline{M}$ the molar mass of the fluid, ρ_v the vapor density and h_{lv} the latent heat of vaporization.

Evaporator and condenser 2D models are solved using the Matlab finite element toolbox. Thermal resistances $R_{th,i,trans}$ are calculated from the resulting temperature field.

2.3 Hydrodynamic model for condensate film thickness calculation

The shape of the condensate film on the fins is calculated with a one-dimensional hydrodynamic model, already presented in Lefèvre *et al.* (2008). We assume that the liquid which condenses on the fins is drained to the grooves following the direction y perpendicular to the grooves. The liquid thickness δ, the liquid pressure P_l and the liquid velocity w_l in the film are calculated along the y axis (Fig. 3). Owing to the symmetries, only one half of the fin is modeled.

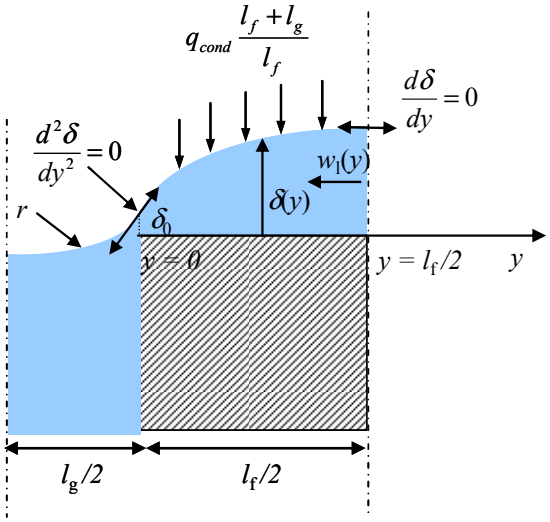

Fig. 3 Condensate film model

The film is divided into several control volumes of length dy for which the balance equations are written for the liquid. The vapor pressure is supposed to be constant and equal to P_v, corresponding to the saturation pressure of the fluid. Condensation is assumed to occur homogeneously on the top of the fins. Thus, the heat flux of condensation is equal to $q_{cond}(l_f+l_g)/l_f$ where l_f and l_g are the fin width and the groove width respectively. The mass balance for the liquid is expressed as:

$$\frac{d(\delta w_l)}{dy} = \frac{1}{\rho_v h_{lv}} q_{cond}\frac{l_f+l_g}{l_f} \quad (4)$$

By neglecting the liquid-vapor interfacial shear stress, the momentum equation is written:

$$\rho_l \frac{d\left(\delta w_l^2\right)}{dy} = -\delta\frac{dP_l}{dy} + \tau_{lw} \quad (5)$$

where τ_{lw} is the liquid-wall shear stress calculated in laminar conditions with a hydraulic diameter for the Reynolds number equal to 2δ. Let us introduce K the liquid-vapor interface film curvature and δ' the derivative of δ with respect to y:

$$K = \frac{\frac{d^2\delta}{dy^2}}{\left(1+\left(\frac{d\delta}{dy}\right)^2\right)^{\frac{3}{2}}} \quad (6)$$

$$\frac{d\delta}{dy} = \delta' \quad (7)$$

By introducing Eq. (7) in Eq. (6), we obtain a first order differential equation:

$$\frac{d\delta'}{dy} = K\left(1+(\delta')^2\right)^{\frac{3}{2}} \quad (8)$$

Owing to the Young-Laplace law, if $K < 0$, the liquid pressure on the fin top is higher than the vapor pressure:

$$P_v - P_l = \sigma K \quad (9)$$

By introducing Eq. (9) in Eq. (8), we obtain:

$$\frac{d\delta'}{dy} = \frac{P_v - P_l}{\sigma}\left(1+(\delta')^2\right)^{\frac{3}{2}} \quad (10)$$

Equations (4), (5), (7) and (10) constitute a set of four coupled first-order differential equations that is solved numerically with a fourth order Runge-Kutta method. The boundary conditions are supposed to be known at the corner of the fin (y=0). The liquid film thickness is supposed equal to δ_0. The energy balance gives the value of the liquid velocity at y=0 since we suppose that all the condensate is drained to the grooves:

$$w_l(0) = \frac{q_{cond}\left(l_f+l_g\right)/2}{\rho_l h_{lv}\delta_0} \quad (11)$$

As the meniscus curvatures in the groove and that on the top fin are in opposite signs, the function $\delta(y)$ has an inflexion point. We assume that this inflexion point is located at y = 0. Thus, the meniscus curvature is equal to zero and the liquid pressure is equal to the vapor pressure at this special point. Finally, the meniscus curvature radius r is supposed to be constant in the grooves, which gives the value of δ' at y=0:

$$\delta'(0) = \frac{l_g}{\sqrt{4r^2 - l_g^2}} \quad (12)$$

A shooting method is used to calculate the value of δ_0, which is obtained when the derivative of δ with respect to y is equal to zero on the fin symmetry axis at $y = l_f/2$.

2.4 Modified thermal model for evaporation and condensation heat transfer estimation

To solve the thermal model, the accommodation coefficient of the working fluid has to be known experimentally. We have shown in a

Global Digital Central
ISSN: 2155-658X

previous article (Lefèvre *et al.*, 2008) that this parameter has a huge influence on the temperature field of the heat pipe. Nevertheless, this coefficient is not well referenced in the literature. As an illustration, the literature review of Marek and Straub (2001) shows a huge dispersion of the experimental results presented in the literature for water. Furthermore, if several references are available for water, few or no results are available for other fluids.

In this article, the model is compared to several experimental results obtained with a FPHP filled with pentane, whose accommodation coefficient is not studied in the literature to our knowledge. In order to analyze the experimental results, the nodal model presented in section 2.1 is compared to experimental temperature measurements, which permits to estimate the saturation temperature and the mean thermal resistances of evaporation and condensation in different experimental conditions. Thus, in the nodal thermal model, $R_{th,\,i,\,trans}$ is supposed to be constant in the condensation area and in the evaporation area. Condensation occurs when the wall temperature T_i is lower than the saturation temperature T_{sat}. Evaporation occurs when $T_i > T_{sat}$. As the FPHP is divided in n nodes, we obtain a set of n equations (see Eq. 1) with n+3 unknowns: n temperatures at each node, the saturation temperature and the mean transversal thermal resistances at the condenser and at the evaporator. The number of temperature sensors is sufficient to perform the parameter estimation. The results are used to calculate the evaporation and condensation heat transfer.

3. EXPERIMENTAL BENCHES

Results obtained with two different FPHPs are presented in this article. Temperature measurements obtained with a FPHP made of copper are compared to the thermal model. Liquid-vapor interface measurements obtained with a second FPHP made of silicon are used to interpret some of the results.

3.1 FPHP made of copper

The flat heat pipe under investigation is shown in Fig. 4. It has already been described in previous articles (Lips et al., 2009 & 2010). The capillary structure, of dimensions 70×90 mm², is made of 88 longitudinal micro-grooves, machined in a copper plate. The grooves are connected at the condenser. Each groove has a rectangular cross-section of height and width equal to 400 µm. The distance between two grooves is equal to 400 µm. The wall thickness under the grooves is equal to 2.6 mm.

The FPHP is hermetically sealed on its upper face with a transparent plate, which allows observations inside the device. The vapor space thickness can vary by changing the thickness of a nitrile flat gasket. The heat source is an electrical resistance in a copper block of dimensions 70 × 20 mm^2 supplied by a 0 - 220 V AC power supply. The heat sink is a water heat exchanger of dimensions 30 × 70 mm^2. The water flow rate is constant and the inlet temperature is controlled by means of a thermostatic bath in order to have a constant working temperature when the heat input increases. The heat source and the heat sink are separated by an adiabatic area of length equal to 40 mm.

3.2 FPHP made of silicon

The flat plate heat pipe made of silicon is shown in Fig. 5. It has been presented in Lefèvre et al. (2010). Its capillary structure, of diameter 50 mm, is etched on a silicon wafer of 100 mm diameter and 525 µm thickness. It is made of 72 radial micro-grooves that are connected by crossed grooves at the centre of the device. The etching depth is equal to 200 µm. The radial grooves have a rectangular cross-section whose width varies from 670 µm at the periphery to 110 µm at the connection with the crossed grooves. These crossed grooves have a width equal to 100 µm and they are separated by fins of same width, which creates a network of 300 small posts of 100 × 100 µm^2. The FPHP is hermetically sealed on its upper face with a borosilicate plate, which allows liquid film measurements by confocal microscopy in the capillary structure. The vapor space thickness is equal to 2 mm.

A circular heat source, made of a thick resistor film of surface 1 cm^2, is located in the middle of the silicon wafer. The heat sink is a circular water heat exchanger (inlet radius of 22 mm and outlet radius of 25 mm; surface equal to 4.4 cm^2).

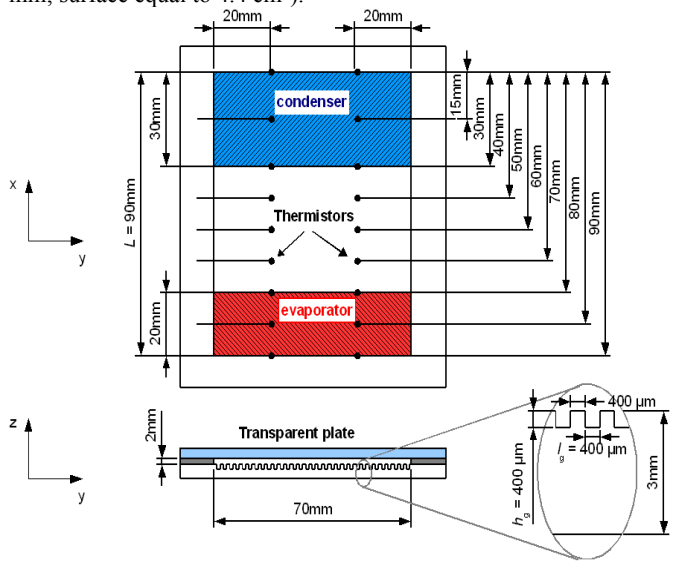

Fig. 4 FPHP made of copper

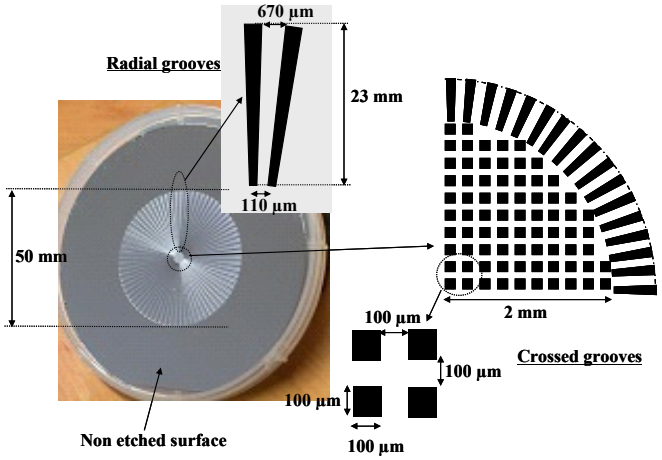

Fig. 5 FPHP made of silicon (Lefèvre *et al.*, 2010)

3.3 Confocal microscopy

Capillary phenomena, evaporation, and condensation in micro channels have been the focus of a lot of experimental studies these last years. In a heat pipe, these phenomena are linked together and cannot be studied separately. Therefore, it is difficult to perform measurements in such a device. For example, micro-PIV is not helpful in heat pipes because the process of insemination is not appropriate. Indeed, any particles introduced in the liquid would be blocked at the evaporator because of their non evaporative character. Among classical techniques for film thickness measurement applied to micro-scale two-phase flow systems, confocal microscopy has appeared to be the most appropriate to characterize FPHPs. More details on this measurement technique can be found in several of our articles, for example in Rullière *et al.* (2007) or Lefèvre *et al.* (2010).

Our confocal microscope is a STIL Micromesure 2 system. The optical sensor has a nominal measuring range of 350 µm. The working distance is about 13 mm. The optical sensor velocity is about 1 mm.s^{-1}, which is fast enough for not thermally disturbing the measurement.

Once the top of the groove is detected by the sensor, the liquid-vapor interface is recorded. The resulting data are used to estimate the curvature of the surface.

Optical principle of confocal microscopy is the following. A white light point source is imaged by a lens that has not been corrected for chromatic aberrations on a series of monochromatic point images in the measurement space. The reflected light passes back through the lens and is directed towards a spectral detector by a partially reflecting mirror. The spectral analysis of the collected rays that are separated by a spatial filter allows the location of the surface to be measured. The monochromatic light having the highest intensity corresponds to the surface to be measured.

4. COMPARISON BETWEEN EXPERIMENTAL RESULTS AND THERMAL MODELS

4.1 Experimental results obtained with the FPHP in copper

The FPHP made of cooper has been studied in a variety of experimental conditions (see table 1), which creates a significant experimental database. Experimental parameters are the vapor space thickness, the inclination angle, the filling ratio and the heat transferred by the system. The filling ratio is defined as the ratio of the volume of liquid to the total volume of the FPHP. For inclination angles of 2.5° and 5°, the FPHP is tilted in unfavorable orientation, i.e. the evaporator higher than the condenser. N-pentane is used as working fluid. Its saturation temperature has been kept equal to 40 °C. In all the experiments, temperatures are recorded as well as the meniscus curvature radius along the grooves measured by confocal microscopy.

The comparison between the temperature fields obtained by the model and experimentally, when the FPHP is empty, is presented in Fig. 6. Different heat transfer rates at the heat source (15 W< Q < 281 W) are tested. The longitudinal thermal resistance is calculated through a parameter estimation method. This resistance is rather constant whatever the heat flux at the heat source: $R_{th,long}$ = 7.5 ± 0.2 $KW^{-1}m^{-1}$. This value is introduced in the thermal model to identify the transversal thermal resistance in working conditions.

Fig. 7 presents a comparison between the temperature fields in working conditions (Q = 28 W) and the model. The FPHP is in horizontal position. The vapor space thickness is equal to 2 mm and the filling ratio equal to 9%. A satisfactory agreement is found between the model and the experimental results. The evaporation and condensation heat transfer that fit at best the experimental results are equal to 1708 $Wm^{-2}K^{-1}$ and 1563 $Wm^{-2}K^{-1}$ respectively.

Table 1 Experimental conditions

Vapor space thickness (mm)	*Inclination angle (°)*	*Filling ratio*	*Heat transfer rate (W)*
1 mm	0	18 %	28
			45
2 mm	0	9 %	28
			45
			88
		13 %	28
			45
			57
			88
	2.5	10 %	44
			59
	5	10 %	28

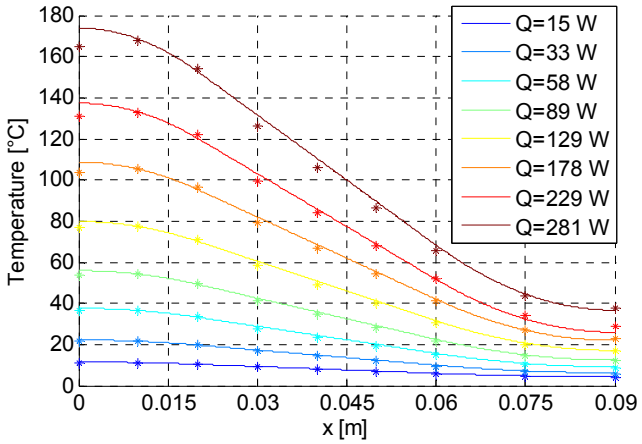

Fig. 6 Measured and calculated temperature fields when the FPHP is empty

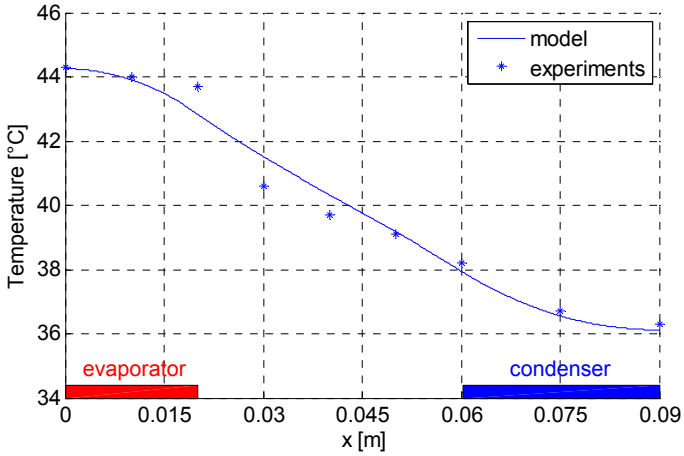

Fig. 7 Measured and calculated temperature fields in working conditions (Q = 28 W)

Fig. 8 presents meniscus curvature radius measurements along the FPHP in the same experimental conditions as in Fig. 7. Uncertainties are given for each measurement. They are not due to the measurement method, but to the dispersion of the meniscus curvature radii in several grooves at the same longitudinal location. Points in Fig. 7 are the mean curvature radius of 12 grooves at a location x and uncertainties have been evaluated with a confidence interval of 95 %.

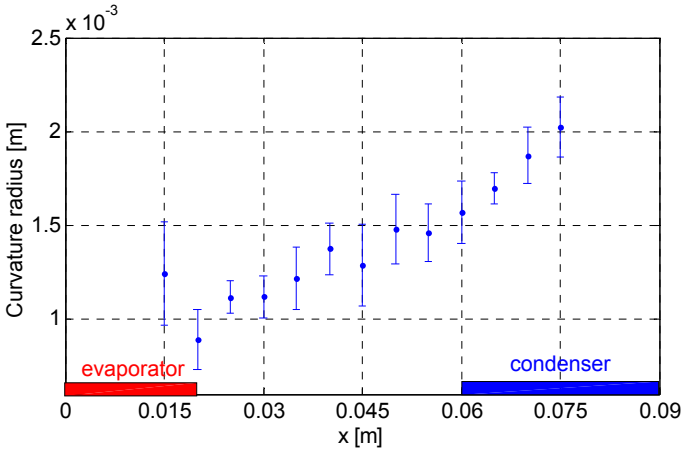

Fig. 8 Measured meniscus curvature radii along the grooves (Q = 28 W)

Global Digital Central
ISSN: 2155-658X

4.2 Comparison with the evaporation model

The evaporation model presented in section 2.2 depends on the shape of the liquid inside the grooves, especially the meniscus curvature radius. It depends also on the accommodation coefficient. Results of the model are presented in Fig.9. In the following sections, we call evaporation and condensation heat transfer coefficients the thermal conductance (i.e. the inverse of the thermal resistance) of the capillary structure filled with the working fluid in the evaporation area and in the condensation area respectively. The evaporation heat transfer coefficient is calculated for different meniscus curvature radii (200 µm $< r <$ 2000 µm) and accommodation coefficient ($0.02 < a_c < 0.16$). On the same figure, heat transfer coefficients estimated by comparison between the thermal model and the experimental results are presented with horizontal lines. These lines represent the range of variation of the meniscus curvature radius in the evaporator during the experiments. The stars represent the mean radius of curvature in the evaporator zone.

We can note that, except for two points, experimental results are in good agreement with numerical results for an accommodation coefficient equal to 0.06±0.02. Unfortunately, we have not found experimental measurements of the accommodation coefficient for pentane, which prevents comparison. The heat transfer coefficient decreases with the increase of the meniscus curvature radius. Indeed, most of the heat flux is transferred at the junction between the meniscus and the fin. Small meniscus curvature radii lead to small liquid film thickness at the junction between the meniscus and the fin, which increases evaporation heat transfer coefficients.

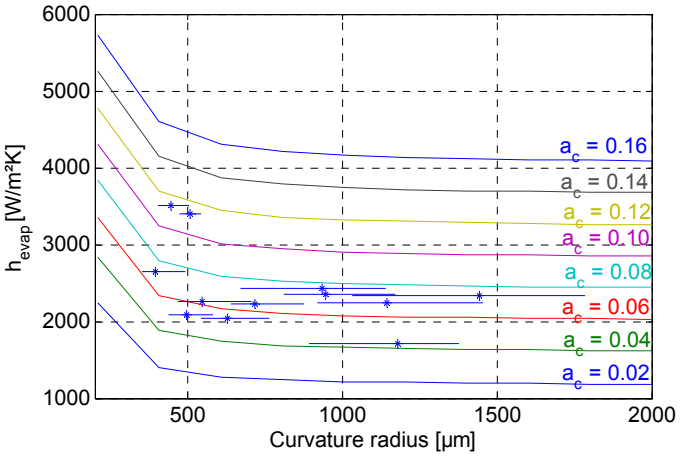

Fig. 9 Calculated and measured evaporation heat transfer coefficients

4.3 Comparison with the condensation model

The condensation model presented in section 2.2 depends on the meniscus curvature radius and the accommodation coefficient like the evaporator model. It depends also on the heat flux of condensation. A comparison with the experimental results is presented in Fig. 10. The condensation heat transfer coefficient is plotted versus the meniscus curvature radius for different condensation heat fluxes (0.5 Wcm$^{-2} < q <$ 4 Wcm^{-2}) and two accommodation coefficients ($a_c = 0.06$ in solid lines and $a_c = 0.01$ in dashed lines). On the same figure, heat transfer coefficients estimated by comparison between the thermal model and the experimental results are presented with horizontal lines. These lines represent the range of variation of the meniscus curvature radius in the condenser during the experiments. The stars represent the mean radius of curvature in the condenser zone.

Contrary to the evaporation model, numerical results are not in agreement with experimental results even with a very small accommodation coefficient. The model overestimates heat transfer coefficients. This result can be partially explained by the fact that a part of the condenser is flooded by the liquid in excess in the system. Nevertheless, one should state that the flooded area, which can be observed in our experiments, is small compared to the condensation area. Thus, it can not explain the huge difference between experimental and numerical results. The lack of accuracy of the model for the liquid film thickness calculation on the top of the fin has to be questioned. Unfortunately, confocal microscopy does not allow condensate shape measurements on the top of the fins. Indeed, copper is too bright and thus the system is not able to focalize on this film. This measurement is feasible on other surfaces, such as silicon. Results are presented in next section.

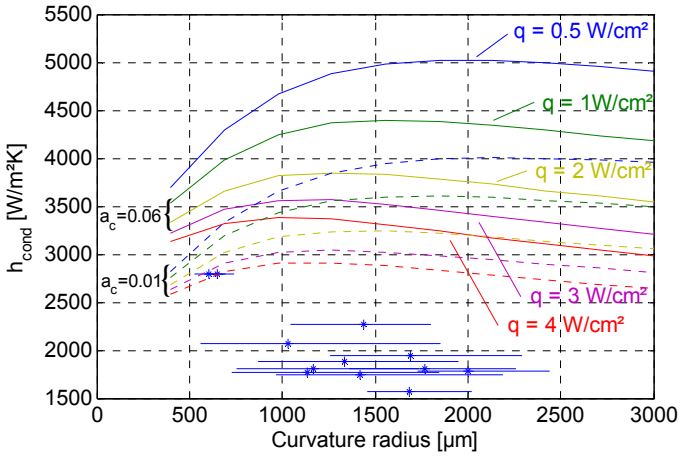

Fig. 10 Calculated and measured condensation heat transfer coefficients

4.4 Condensate film on the fins

Fig. 11 presents the shape of the liquid-vapour interface calculated by the hydrodynamic model (see section 2.3) for 3 different condensation heat fluxes ($q = 1$ Wcm^{-2}, $q = 2$ Wcm^{-2} and $q = 4$ Wcm^{-2}). The width of the fins and the grooves are both equal to 400 µm, like the FPHP made of copper. The thickness of the liquid film at the corner of the fin δ_0 increases with the increase of the heat flux, which is due to the increase of the mass flow rate. However, the shape of the liquid-vapor interface does not change significantly and depends strongly on the meniscus curvature in the groove.

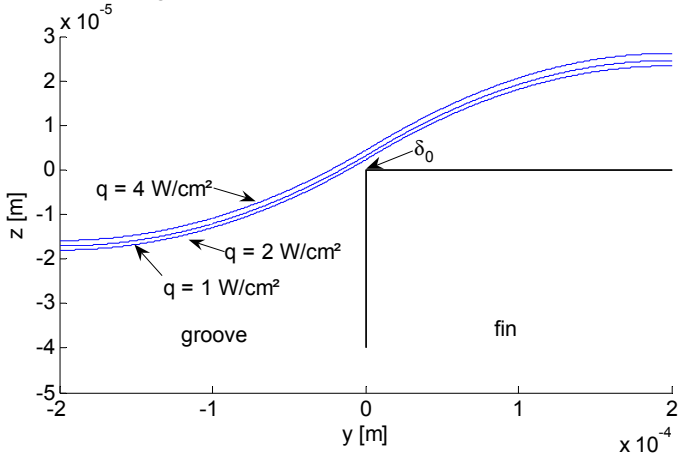

Fig. 11 Calculated liquid-vapor interface shape

Fig. 12 presents the liquid-vapor interface measured experimentally by confocal microscopy in a cross section located in the middle of the condenser (see Lefèvre *et al.*, 2010) of the FPHP made of silicon. The FPHP is filled with methanol with a filling ratio of 4.7%. The heat flux is equal to 8.4 W/cm² and the working temperature is equal to 30 °C. Two grooves are visualized. The width of the grooves and the fins are equal to 400 µm and 800 µm, respectively. Circles that fit the experimental data are plotted on the figure so as to determine the film radii of curvature. One has to notice that the scale on the *y* axis is

Global Digital Central
ISSN: 2155-658X

100 times lower than that on the *x* axis. The radius of curvature is found to be 1.08 mm in the grooves and 12.4 mm on the fins. The thickness of the condensate on the fins is about 5 µm.

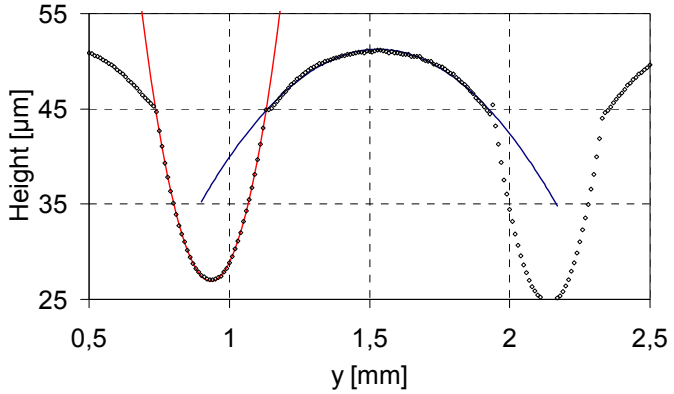

Fig. 12 Experimental liquid-vapor interface shape (Lefèvre *et al.*, 2010)

Fig. 13 presents a comparison between the experimental and the numerical interface shapes. The two profiles are not in good agreement on the top of the fin. Experimentally, a slope break is noticeable between the liquid in the grooves and the condensate on the fins. This observation is not consistent with one of the assumptions of the numerical model, namely that there exists an inflexion point between the meniscus in the grooves and the condensate film.

Lefèvre *et al.* (2010) measured the meniscus curvature radius and the condensate curvature radius from the evaporator to the condenser for different condensation heat fluxes (q = 4.4 Wcm^{-2}, q = 6.4 Wcm^{-2} and q = 8.4 Wcm^{-2}). These experimental results are presented in Fig. 14. Theoretical curvature radii predicted by the model on the top of the fins are plotted in dashed lines. The model underestimates systematically the meniscus curvature radius on the fins. This can lead to an underestimation of the heat transfer coefficient by the model, due to the overestimation of the liquid film thickness. On the contrary, it can also lead to an overestimation of the heat transfer coefficient if the model underestimates the liquid film thickness δ_0 at the corner of the film. Unfortunately, the confocal microscope does not allow measuring precisely both the position of the liquid-vapor interface and the position of the top of the fin simultaneously.

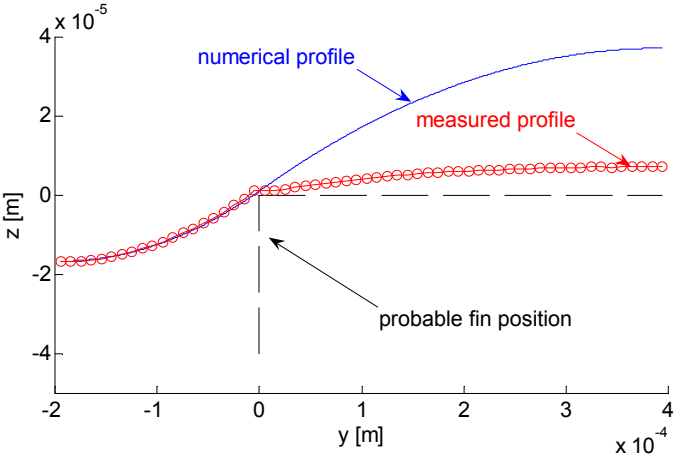

Fig. 13 Comparison between numerical and experimental liquid-vapor interface shape

The experimental results show that a new hydrodynamic model has to be developed to calculate the shape of the liquid film on the fins. Such a model should include a slope break between the liquid in the grooves and the liquid on the fins. By analyzing the results of the theoretical film of condensation, one can observe that the curvature radius on the fins is very close to that of a circle. The pressure drop in the liquid film is too small to deform the drop shape. As a result, a similar result would have been obtained considering only fin and groove widths: the ratio between the curvature radii in the grooves and on the fins is equal to the ratio of the widths of the grooves and the fins. The hydrodynamic model, which is conceived to determine very precisely the shape of the liquid film on the fins, has for result a circle that can be calculated easily by geometrical considerations.

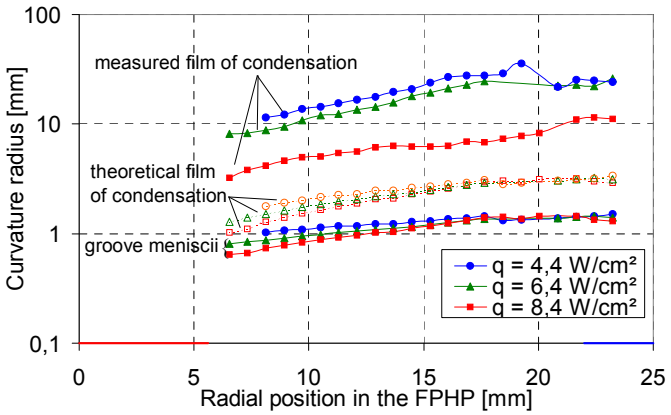

Fig. 14 Comparison between numerical and experimental liquid-vapor interface shapes

The development of a new hydrodynamic model should focus on the presence of a slope break between the liquid in the groove and on the fins. Two assumptions can explain this slope break. Either there is a junction between the two liquid films, which permits the liquid to be drained from the fins to the grooves, or this junction does not exist and thus the condensate is not drained perpendicularly to the grooves but parallel to the grooves.

The first assumption can be justified if the slope break is just a macroscopic view of a very small zone where the variation of the curvature radius is so high that it can change the curvature orientation. This small region would be located at the edge of the fins where the liquid film thickness is small enough to generate high pressure drops. The future model would then be similar to the current model but it has to be developed for a much smaller region at the junction between the liquid in the groove and the liquid on the fins. Van der Waals forces could be included if the film thickness is very small.

The second assumption seems to be in agreement with the experimental results presented in Fig. 14. Indeed, if the liquid is drained parallel to the grooves, the pressure of the liquid should vary on the fins. This is the case in the experiments since the measured curvature increases from the evaporator to the condenser, like in the grooves (see Fig. 14). As the curvature in the grooves and the fins are reversed, the liquid on the fins and in the grooves are in counterflow. Thus, the condensate could be drained to the periphery of the FPHP where it would enter the grooves. However, one should noticed that the fin width increases from the center to the periphery of the silicon FPHP too, which can also explain the reason why the curvature on the fins decreases. A new experiment, designed specifically to understand how condensation film are formed, has to be realized.

For both assumptions, more fundamental experimental and theoretical studies are necessary in order to lead to a better understanding on condensation flows in a capillary structure made of grooves and to the development of accurate numerical models.

5. CONCLUSIONS

Temperature measurements and liquid-vapor interface measurements obtained by confocal microscopy have been presented and analyzed

using models of the evaporator and the condenser of a FPHP, which were developed and partially validated in a previous work. A satisfactory agreement is found between the evaporation model and the experiments, for a unique value of the accommodation coefficient. However, the results show that a new approach has to be developed to model the film of condensation. Assumptions have been formulated to enhance this model.

Confocal microscopy allows measuring the liquid-vapor interface shape in the grooves but also on the fins in particular experimental conditions. Even though the knowledge of this interface shape is necessary to model both the evaporator and the condenser, it is not sufficient given that the results are highly dependant to the accommodation coefficient. Since few experimental articles on this coefficient are available in the literature, more studies are required to get an accurate value of the accommodation coefficient for pentane and for others fluids.

ACKNOWLEDGEMENTS

This work was supported by the GIP-ANR in the frame of the non-thematic project ‘‘INTENSIFILM” N° ANR-06-BLAN-0119-03.

NOMENCLATURE

a_c	accommodation coefficient
h	heat transfer coefficient ($Wm^{-2}K^{-1}$)
h_{lv}	latent heat of phase change ($J.kg^{-1}$)
K	curvature (m^{-1})
l	width (m)
L	length (m)
$\overline{M}$	molar mass ($kg.mol^{-1}$)
n	number of nodes
P	pressure (Pa)
q	heat flux ($W.m^{-2}$)
Q	heat transfer rate (W)
r	meniscus curvature radius (m)
R_g	specific gas constant ($J.kg^{-1}K^{-1}$)
R_{th}	thermal resistance ($Km^2.W^{-1}$)
S	surface (m^2)
T	temperature (K)
w	velocity ($m.s^{-1}$)
x,y,z	coordinates (m)

Greek Symbols

δ	liquid thickness (m)
ρ	density ($kg.m^{-3}$)
σ	surface tension (Nm^{-1})
τ	shear stress (Nm^{-2})

Subscripts

0	initial condition
cond	condenser
evap	evaporator
f	fin
g	groove
l	liquid
long	longitudinal
i	node number
trans	transversal
sat	saturation
v	vapor
w	wall

REFERENCES

Carey, V.P., 1992, *Liquid-vapor phase-change phenomena*, Taylor and Francis, London.

Khrustalev, D., Faghri, A., 1994, “Thermal analysis of a micro heat pipe”, *Journal of Heat transfer*, **116**, 189-198.
doi:10.1115/1.2910855

Khrustalev, D., Faghri, A., 1995, “Thermal characteristics of conventional and flat miniature axially grooved heat pipes”, Journal of Heat transfer, **117**, 1048-1054.
doi:10.1115/1.2836280

Khrustalev, D., Faghri, A., 1999, “Coupled liquid and vapor flow in miniature passages with micro grooves”, *Journal of Heat Transfer*, **121**, 729-733.
doi:10.1115/1.2826042

Kim, S.J., Seo, J.K., Do, K.H., 2003, “Analytical and experimental investigation on the operational characteristics and the thermal optimization of a miniature heat pipe with a grooved wick structure”, *International Journal of Heat and Mass Transfer,* **46**, 2051-2063.
doi:10.1016/S0017-9310(02)00504-5

Lallemand, M., Lefèvre, F., 2004, “Micro/mini heat pipes for the cooling of electronic devices”, *Proceedings of 13th International Heat Pipe Conference*, Shanghai, China.

Lefèvre, F., Rullière, R., Pandraud, G., Lallemand, M., 2008, “Prediction of the temperature field in flat plate heat pipes with micro-grooves – Experimental validation”, *International Journal of Heat and Mass Transfer*, **51**, 4083-4094.
doi:10.1016/j.ijheatmasstransfer.2007.12.007

Lefèvre, F., Rullière, R., Lips, S., Bonjour, J., 2010, “Confocal microscopy applied to capillary film measurements in a radial flat plate heat pipe made of silicon”, *Journal of Heat Transfer*, **132**(3), 031502
doi:10.1115/1.4000057

Lips, S., Lefèvre F., Bonjour J., 2009, “Nucleate boiling in a flat grooved heat pipe”, *International. Journal of Thermal Science*, **48**, 1272-1278.
doi:10.1016/j.ijthermalsci.2008.11.011

Lips, S., Lefèvre, F., Bonjour, J., 2010, “Combined effects of the filling ratio and the vapour space thickness on the performance of a flat plate heat pipe”, *International Journal of Heat and Mass Transfer*, **53**, 1113-1121.
doi:10.1016/j.ijheatmasstransfer.2009.10.022

Longtin, J.P., Badran, B., Gerner, M., 1994, “A one-dimensional model of a micro heat pipe during steady-state operation”, *Journal of Heat Transfer*, **116**, 709-715.
doi:10.1115/1.2910926

Marek, R., Straub, J., 2001, “Analysis of the evaporation coefficient and the condensation coefficient of water”, *International Journal of Heat and Mass Transfer*, **44**, 39-53.
doi:10.1016/S0017-9310(00)00086-7

Rullière, R., Lefèvre, F., Lallemand, M., 2007, “Prediction of the maximum heat transfer capability of two-phase heat spreaders - Experimental validation”, *International Journal of Heat and Mass Transfer*, **50**, 1255-1262.
doi:10.1016/j.ijheatmasstransfer.2006.09.015

Vasiliev, L.L., 2008, “Micro and miniature heat pipes – Electronic component coolers”, *Applied Thermal Engineering*, **28**, 266–273
doi:10.1016/j.applthermaleng.2006.02